Nonlinear optical measurements using a 4*f* coherent imaging system with phase objects

G. Boudebs* and S. Cherukulappurath
Laboratoire des Propriétés Optiques des Matériaux et Applications, UMR CNRS 6136, Université d'Angers, 2 Boulevard Lavoisier, 49045 Angers Cedex 01, France
(Received 11 November 2003; published 18 May 2004)

We report a one-laser-shot measurement technique using a phase object at the entry of a 4*f* coherent imaging system to characterize the value of the nonlinear refractive index of materials placed in the Fourier plane of the setup. Experimental and simulated images are presented here in order to validate our approach. We show that the use of a quarter-wavelength dephasing object maximizes the transmission variations in the detected image. We show also that the use of phase objects increases significantly the sensitivity of the measurement compared to top-hat beams (by a factor of 6). Moreover, by adding this type of object at the entry of our imaging system it is possible to determine the sign of the refractive nonlinearity.

DOI: 10.1103/PhysRevA.69.053813 PACS number(s): 42.65.−k, 42.30.Kq

I. INTRODUCTION

We have reported recently a nonlinear-imaging one-laser-shot technique (NIT) based on a 4*f* coherent imager system with top-hat beams to characterize nonlinear optical properties [1]. In this method (see Fig. 1) we studied the Fraunhofer-diffracted image intensity profile. The self-diffracted spectrum on the spatial filter (phase and/or amplitude created by the incident spectrum intensity into the nonlinear material) gives rise to changes in the transmitted intensity. Instead of "*Z* scanning" the material [2] we focused our attention on the transverse modification in the image acquired with a charge-coupled device (CCD) camera. The experimental acquisitions were fitted by a simple theoretical model based on Fourier optics to obtain the nonlinear coefficient. Furthermore, it was shown that the use of top-hat beams instead of Gaussian ones in the 4*f* system increased the sensitivity of the measurements, as was reported by Zhao *et al.* using a *Z*-scan technique [3]. On the other side, we had investigated, both experimentally and theoretically, the optical nonlinearities of infrared chalcogenide glasses using a spatially resolved Mach-Zehnder technique (MZT) [4–7]. Experimental data clearly indicate that the samples used in our experiment cannot be described with the usual third-order nonlinear theory and intensity-dependant nonlinear coefficients were attributed to the presence of fifth-order nonlinear susceptibility [7]. The MZT is a powerful method to obtain one-laser-shot measurements, giving more convincing results when one is looking for intensity-dependant nonlinear coefficients. But the great inconvenience of this technique is the complexity of the optical setup, especially when one is using an unstable beam output [such as from an optical parametric generator (OPG)]. For the NIT method, the alignment is simple. Other advantages included no displacement of the nonlinear medium. However, an inconvenience of this method compared to the *Z*-scan technique or MZT is that we were not able, up to now, to have the sign of the nonlinear index coefficient.

We will show here that, by adding a quarter-wavelength phase objects in the 4*f* imaging system, it is possible (i) to extract the nonlinear optical index of the material with only one-laser-shot, (ii) to increase the sensitivity of the measurement compared with Gaussian or top-hat beam objects, and (iii) to determine the sign of the nonlinear index. We consider CS_2, the well-known nonlinear material, in order to validate this new approach.

In summary, in this paper, we will inverse the Zernike spatial filtering experiment: instead of placing the quarter-wavelength plate in Fourier plane to have information about the unknown phase object at the entry of the imaging system, we will place it in the object plane in order to obtain information on the nonlinear filter induced in the material placed in the Fourier plane.

The theoretical model used for our calculations is briefly recalled in Sec. II. Section III deals with the numerical simulation. Section IV is devoted to the experimental details and results.

II. THEORETICAL MODEL

In this section we briefly recall the adopted theoretical model (see Refs. [1,8,9] for more details). In what follows, it is assumed that Fourier optics is sufficient to describe image formation using the 4*f* system [10].

A two-dimensional object (Fig. 1) is illuminated at normal incidence by a linearly polarized monochromatic plane wave **(**defined by $E=E_0(t)\exp[-j(\omega t-kz)]+\text{c.c.}$, where ω is the angular frequency, k is the wave vector, and $E_0(t)$ is the amplitude of the electric field containing the temporal envelope of the laser pulse**)** delivered by a pulsed laser. Using the slowly varying envelope approximation (SVEA) to describe the propagation of the electric field in the nonlinear medium [11] and since we are concerned with the image intensity, the temporal terms will be omitted. Moreover, thermo-optical effects are not significant when one is using ultrashort pulses in the picosecond range (the full width at half maximum time τ is 15 ps) and low repetition rate (10 Hz). If the transmittance of the object is $t(x,y)$, the field amplitude in the focal

*Corresponding author. FAX: (33) (0)2.41.73.52.16. Electronic address: georges.boudebs@univ-angers.fr

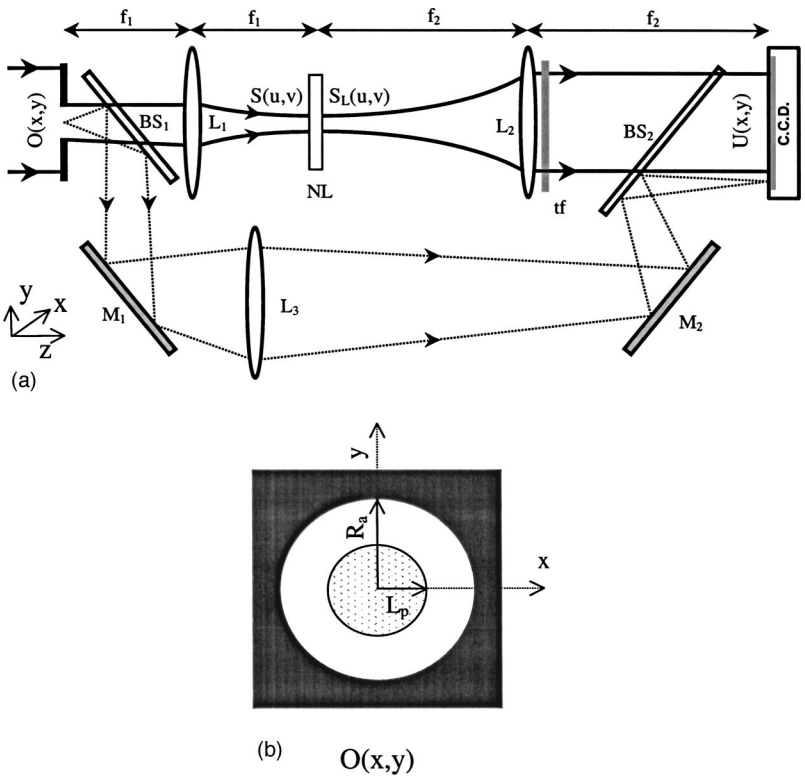

FIG. 1. (a) Schematic of $4f$ coherent system imager. The nonlinear material (NL) is placed in the Fourier plane. L_1–L_3, lenses; M_1, M_2, mirrors; BS_1, beam splitter; tf, neutral filter. (b) Schematic of phase object used at the entry of the setup.

plane of the first lens L_1 is the spatial Fourier transform of $O(x,y)=Et(x,y)$:

$$S(u,v) = \frac{1}{\lambda f_1}\tilde{\mathcal{F}}[O(x,y)] = \frac{1}{\lambda f_1}\int\int O(x,y)\exp[-2\pi j(ux+vy)]dx\,dy, \quad (1)$$

where $\tilde{\mathcal{F}}$ denotes the Fourier transform operation, $u=x/\lambda f_1$ and $v=y/\lambda f_1$ are the spatial frequencies in the focal plane, f_1 is the focal length of the lens L_1, and λ is the wavelength of the exciting wave.

At the output of the $4f$ system, the image intensity can be written as

$$I_{\text{im}}(x,y) = |U(x,y)|^2 = \left|\tilde{\mathcal{F}}^{-1}[S(u,v)T(u,v)H(u,v)]\right|^2, \quad (2)$$

where $\tilde{\mathcal{F}}^{-1}$ denotes the inverse Fourier transform and $H(u,v)$ the coherent optical transfer function applicable to aberration-free lenses, $H(u,v)=\mathfrak{C}(\sqrt{u^2+v^2}\lambda G/N_A)$. The function $\mathfrak{C}(\rho)$ is defined equal to 1 if the radius $\rho(u,v)$ is less than or equal to 1 and 0 elsewhere. N_A is the numerical aperture of the lens L_1 and G is the magnification of the optical system. We assume a cubic nonlinearity and we consider samples exhibiting (i) linear absorption defined by α (m^{-1}), (ii) two-photon absorption (2PA) defined by β (m/W), and (iii) a nonlinear index defined by n_2 (m^2/W). When the nonlinear medium is regarded as "thin," the complex field at the exit face of the sample can be written [12]

$$S_L(u,v) = S(u,v)e^{-\alpha L/2}[1+q(u,v)]^{(jkn_2/\beta-1/2)}, \quad (3)$$

where $q(u,v)=\beta L_{\text{eff}}I(u,v)$, $L_{\text{eff}}=(1-e^{-\alpha L})/\alpha$, L is the sample length, and $I(u,v)$ denotes the intensity of the laser beam within the sample (proportional to $|S(u,v)|^2$). $T(u,v)$, the complex amplitude response introduced by nonlinearity, is defined as

$$T(u,v) = \frac{S_L(u,v)}{S(u,v)} = \{e^{\alpha L}[1+q(u,v)]\}^{-1/2}\exp[j\varphi_{\text{NL}}(u,v)], \quad (4)$$

where φ_{NL}, the nonlinear phase shift of the beam, is given by

$$\varphi_{\text{NL}}(u,v) = \frac{kn_2}{\beta}Ln[1+q(u,v)]. \quad (5)$$

In the particular case of a lossless Kerr material, where α and β are both negligible (such as CS_2 considered hereafter in Secs. III and IV), Eq. (5) reduces to $\varphi_{\text{NL}}(u,v)=kn_2LI(u,v)$ and Eq. (3) to $S_L(u,v)=S(u,v)\exp[j\varphi_{\text{NL}}(u,v)]$ [2].

By considering a top-hat beam experiment, a circular diaphragm at the entry of $4f$ setup defines the object with transmittance

$$t_a(x,y) = \mathfrak{C}[\sqrt{x^2+y^2}/R_a]. \quad (6)$$

This assumption is valid only if R_a, the radius of the aperture, is much smaller compared to the spatial extension of the incident beam (i.e., beam waist of the Gaussian beam) in order to assume an incident plane wave passing through the aperture. Let us now add a circular phase object of radius

$L_p(L_p<R_a)$ centered inside the top-hat beam having a uniform phase shift ϕ_L. The transmittance of this new object can be written [see Fig. 1(b)]

$$t_p(x,y) = t_a(x,y)\exp\{j\phi_L \mathfrak{C}[\sqrt{x^2+y^2}/L_p]\}. \quad (7)$$

In the focal plane of lens L_1 the intensity pattern distribution (which becomes the Airy pattern distribution when the phase object is absent—i.e., $L_p=0$ or $L_p>R_a$) induces amplitude and/or phase circular grating in the material (NL). The self-diffracted spectrum on this pattern is collected by the second lens (L_2). Thus in the image plane we obtain a spatially filtered image of the circular phase object having intensity profile variations.

III. NUMERICAL SIMULATION

In order to illustrate the validity of this model, numerical simulations have been compared to experimental acquisitions in Ref. [1] (where the phase object was absent) and compared with some experimental results found in the literature such as in [13,14]. Very good agreement was obtained between acquired and calculated images which allowed us to measure the absolute value of the nonlinear index corresponding to CS_2 and to estimate the n_2 coefficient of different chalcogenide glasses. In this paper, we added a circular phase object defined by Eq. (7). In Fig. 2, we can see the calculated images using our model [Eqs. (1)–(7)] for ϕ_L, the phase shift in the object equal to $\pi/2$. The other parameters of the simulation are close to those found in the experiment (detailed below): $I_0=4.8$ GW/cm^2, $\lambda=1.06$ μm, $L=1$ mm, $\beta=0$, $n_2=3.2\times10^{-18}$ m^2/W, $L_p=0.5$ mm, $R_a=1.45$ mm, $N_A=0.1$, and $G=1$. The x and y coordinates are in pixels (12×12 μm^2). The left image (1) is obtained without the phase object and the right one (2) is the image in the presence of the quarter-phase plate. Note the increasing of the transmitted intensity inside the geometrical image of the phase plate. As shown in this figure, the transmission change ΔT (defined as the difference between the mean values of the diffracted intensity inside the phase plate and the intensity outside) is considerably increased. The whole energy in the image should be conserved (because there is no absorption); therefore, we can see from Fig. 2(b) by comparing profiles (1) and (2) that the increased intensity in the center is deflected from outside the wave plate. Inversely, for negative n_2 and by considering the same parameters as before, the simulation gives profile (3) in Fig. 2(c), where we can see a decrease in the intensity profile at the center to the benefit of the region outside the phase plate. Physically, this behavior can be understood by considering a constructive or destructive interference between the filtered spatial frequencies forming the image depending on the sign of the nonlinear dephasing (i.e., the sign of n_2). In Zernike phase contrast microscopy such a behavior is well known and is called "positive or negative phase contrast" (p. 221 of Ref. [10]). This is an important result because it is the first time to our knowledge that we are able to characterize the sign of n_2 with an only one-laser-shot diffraction-based technique.

A numerical simulation was performed in order to find the best parameters L_p and ϕ_L of the phase object that gives the maximum of ΔT. The parameters of the simulation were $I_0=0.96$ GW/cm^2 (at $\phi_L=0$), $\lambda=1.06$ μm, $L=1$ mm, $\beta=0$, $n_2=3.2\times10^{-18}$ m^2/W, $R_a=1.45$ mm, and $G=1$. Here $H(u,v)$, the coherent optical transfer function, is considered to be very large in order to avoid the "ringing" effect that occurs at the edge transition. The results are shown in Fig. 3 where we can see that ϕ_L giving the ΔT maximum depends on the radius L_p. However, the phase plate that has been used in our experimental acquisitions here below ($L_p=0.5$ mm) shows approximately a maximum around $\phi_L=\pi/2$. In Fig. 4 we calculated the transmission change as a function of $\varphi_{\mathrm{NL\ max}}$, the nonlinear phase shift at the center of the incident spectrum beam. Note the good linearity between ΔT and $\varphi_{\mathrm{NL\ max}}$. The sensitivity, as indicated by the slope of linear lines, increases slowly for a lower radius of the phase object. It should be mentioned here that the sensitivity increases approximately by a factor of 6 when we compare the dotted lines (phase objects of different radius) with the solid one (no phase shift in the object).

IV. EXPERIMENTAL RESULTS AND DISCUSSION

Excitation is provided by a Nd:YAG laser (continuum) delivering 15-ps single pulses at $\lambda=1.064$ μm with 10-Hz repetition rate. The input intensity is varied by means of a half-wave plate and a Glan prism, in order to maintain linear polarization. A beam splitter at the entry of the setup [Fig. 1(a)] permits one to monitor any fluctuation occurring in the incident laser beam. Other experimental parameters are $f_1=f_2=30$ cm (focal length of lenses L_1 and L_2), $G=1$, and $R_a=1.4$ mm. The latter is small compared to the beam waist of the incident laser beam (1 cm). The Airy radius at the focal plane of lens L_1 is $\omega_0=1.22\lambda f_1/(2R_a)=140$ μm giving a Rayleigh range $z_0=\pi\omega_0^2/\lambda\approx6$ cm. This value is much larger than specimen thickness (1-mm-thick fused silica cell). The image receiver is a (1000×1018)-pixel cooled camera (Hamamatsu C4880) with a fixed linear gain. The camera pixels have 4095 gray levels. Neutral filters (such as tf) are used to keep the camera within its linear response range. The phase-changing circular plate consists of a glass structure on which a transparent dielectric disk (of radius $L_p=0.5$ mm) has been deposited [Fig. 1(b)]. The disk has a thickness and index of refraction such that it retards the phase of the incident light by $\pi/2$ radians relative to the phase outside the disk. We verified that the phase shift in the object is independent of the direction of the incident rectilinear polarized beam. By rotating the phase plate we could not observe any significant change in the acquired image, neither in the linear regime nor in the nonlinear one.

Three sets of acquisitions are needed. (i) *No material*: the first acquisition is made without the nonlinear material. This acquisition is used to calibrate the incident intensity in the Fourier plane. We perform a two-dimensional spatial fast Fourier transform (FFT) on the image and compare its spectral density to the energy given by a calibrated joulemeter. Thus, for each laser shot, we are able to monitor the energy and spatial profile fluctuations by reading the image of the reference beam given by lens L_3 (after another calibration of the reference compared with the joulemeter). Here we as-

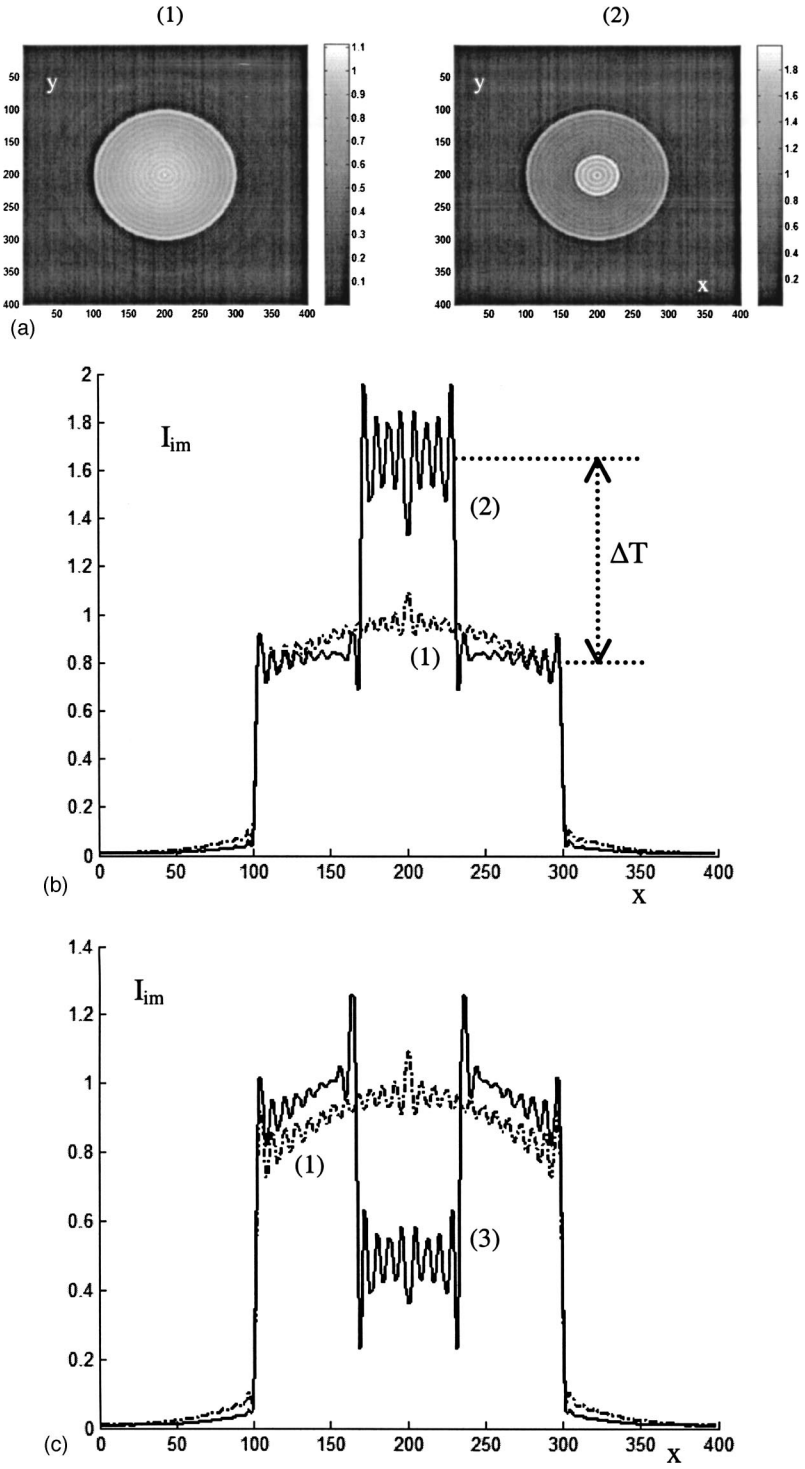

FIG. 2. (a) Numerical simulation of the top-hat beam images at the output of the $4f$ setup after transmission through CS_2; the left image (1) is obtained without the phase object and the right one (2) is the image with the phase object ($\phi_L = \pi/2$). (b) The solid and dotted lines below are the profiles of images (1) and (2). The numerical parameters are the same than those used in Fig. 2(a). (c) Numerical simulation of the image profiles for negative n_2 ($n_2 = -3.2 \times 10^{-18}$ m^2/W). The other parameters are the same as in (a). Note the loss of the transmitted intensity inside the geometrical image of the phase object characterizing a negative nonlinear phase shift due to negative n_2 [profile (3)].

sume that temporal pulse duration is constant and is always equal to 15 ps. (ii) *Linear acquisition* [see Fig. 5(a)]: the second acquisition is done with low incident intensity by placing high-density neutral filters (tf) before the nonlinear medium (NL). In order to define $t_p(x,y)$, the transmittance of the object, the location of the physical edges of both the top-hat beam, and the phase plate are needed. For the top-hat beam, we find all the pixels under 25% of the mean asymptotic value intensity distribution inside the aperture and we put them to zero (see p. 159, Ref. [10]). For the phase plate object, we consider the minimum of the intensity that occurs after diffraction on the step phase. (iii) *Nonlinear acquisition* [see Fig. 5(b)]: the final acquisition is carried out by placing the same high-density neutral filters (tf), used before, after the nonlinear material. This acquisition will be used to deduce the n_2 value by comparison with the theoretically calculated image given by relations (1)–(7) in Sec. II. As predicted by the theoretical calculations (in Sec. III) we note the increasing of the phase contrast inside the phase plate.

The comparison between the experimental nonlinearly filtered image [Fig. 5(b)] and its numerical simulation using the model described above taking into account the previously

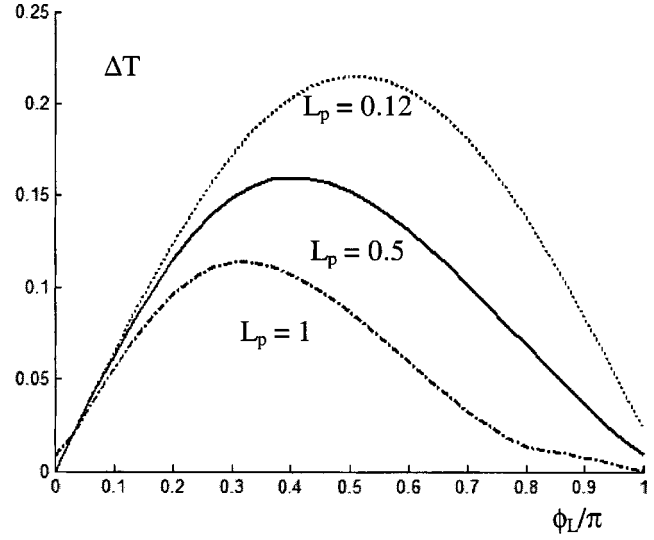

FIG. 3. Calculated transmission changes (ΔT) for different radius L_p (given in mm inside) as a function of the phase shift in the object.

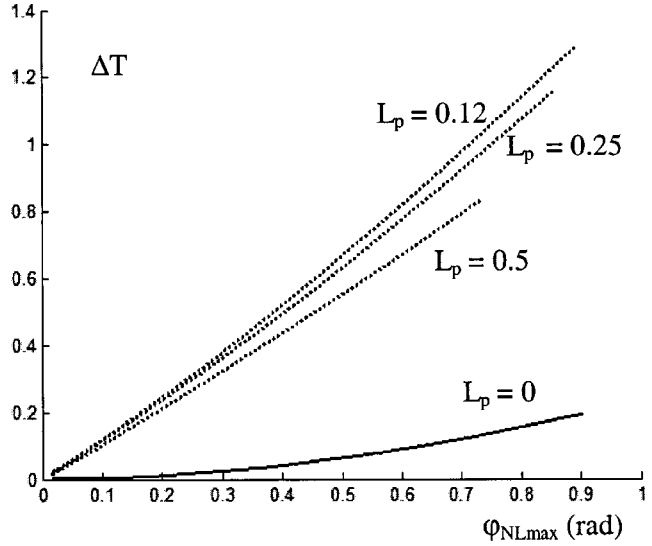

FIG. 4. ΔT as a function of the maximum induced nonlinear phase shift for different values of the radius L_p (given in mm inside this figure).

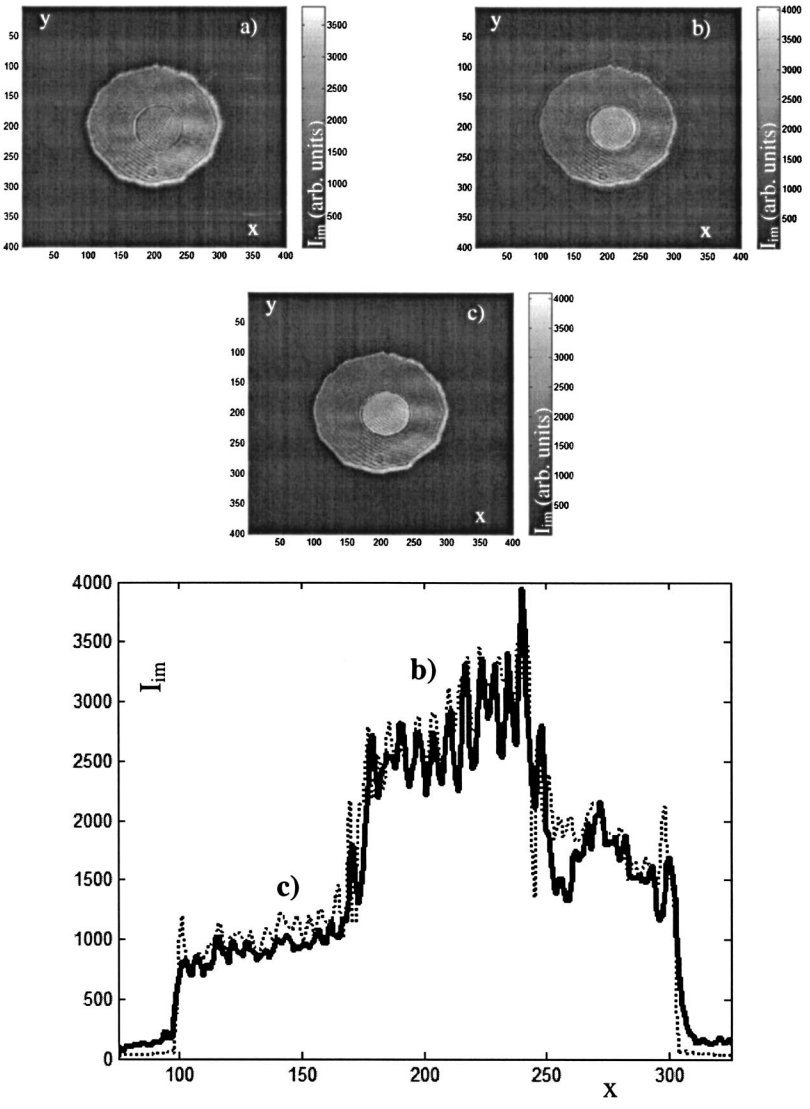

FIG. 5. (a) Experimental acquisition showing the image of the phase object inside the aperture at the entry of the setup under low incident intensity. Note the diffraction that occurs at the border of the circular phase plate. (b) Experimental acquisition showing the image of the phase plate at the entry of the setup under high incident intensity ($I_0 = 3.8$ GW/cm^2) through 1-mm-thick CS_2. Note the increasing of the phase contrast inside the circular phase object. (c) Theoretical simulation of the image given by the measured optimized n_2 value ($n_2 = 3.2 \times 10^{-18}$ m^2/W) found by fitting the experimental acquisition in (b) using our model. (d) Profiles of images (b) and (c) taken at $y = 200$. The comparison of profiles (b) (in bold) and (c) (dots) shows a very good agreement between experimental acquisition and numerical simulation.

defined object by "linear acquisition" leads to the knowledge of the nonlinear characteristics of the filtering material. This is done by fitting the calculated image to the experimental one by varying n_2, the only unknown parameter in relations (2) and (4). All the other parameters in these relations are supposed to be known ($I_0=3.8\ \mathrm{GW/cm^2}$, $L=1$ mm, $\alpha=0$, $\beta=0.8$ cm/GW, $N_A=0.1$, $\lambda=1.064\ \mu$m, $G=1$, $R_a=1.4$ mm, $L_p=0.5$ mm). We have used the subroutine fminsearch of Matlab which uses the Nelder-Mead simplex (direct search) method for unconstrained nonlinear minimization. We can see in Fig. 5(c) the theoretical simulation of the image given by the measured absolute n_2 value ($n_2=3.2\times10^{-18}\ \mathrm{m^2/W}$) obtained from fitting. This fitting has been done for ten different sets of acquisitions showing a good reproducibility of the measurements (within 10% error). In Fig. 5(d)) we show the profiles of the experimental and simulated images along an axis passing through the center the aperture. As can be noted, very good agreement is found between theory and experiment. Moreover, the absolute value obtained with our good lossless Kerr medium (CS_2) is very close to values found in the literature [1,2,4,6,8,13,14].

It is interesting to note the analogy that exists between our *XY*-scan experiment done here (using transmission changes in the transverse plane containing the CCD) and the usual *Z* scan (using transmission changes in the longitudinal axis). Furthermore, the use of the closed aperture in the *Z*-scan-normalized transmittance to detect the refractive nonlinearity should be compared with the use of the circular phase plate in this paper. Indeed, Fig. 4 here shows an increase of the sensitivity with lower radius of the phase plate which is analogous to the increase of sensitivity in *Z* scan with lower aperture size (see Fig. 3 in Ref. [2]). Moreover, in both cases, the measured signal (ΔT here, peak-valley difference in *Z* scan) is proportional to the induced nonlinear phase shift. Another analogy comes from the fact that in both techniques we are able to determine the sign of n_2 from a positive or a negative transmission change. So, finally, the advantage of the *XY* scan is that all this information is obtained with only one-laser-shot profiting from the parallelism inherent to coherent optical information processing $4f$ systems.

Finally, the question that remains is, should we expect an increasing of the sensitivity with the usual *Z*-scan experiment by adding a phase object at the entry of the setup? We believe yes. Experiments and simulations in this regard are underway. It will be very useful to add a simple quarter-phase object in the existing conventional *Z*-scan experiments to improve the sensitivity of the measurement for those who do not want to use a CCD camera.

V. CONCLUSION

In this paper we have reported a powerful but simple technique based on nonlinear imaging with a top-hat beam associated with a quarter-wavelength phase object to characterize the nonlinear refractive index. First we showed numerically that phase objects are preferable to amplitude ones, especially for determining the sign of n_2. Next we showed that the sensitivity is increased by a factor of 6 compared to the use of top-hat beams. In order to validate the method, we measured the nonlinear coefficient of CS_2. The absolute value obtained is in very good agreement with other results obtained by different methods. The optical alignment is easy and no displacement of the material is needed unlike in the *Z*-scan method. Only one-laser-shot is required, giving the possibility to study materials showing intensity-dependant n_2. On the other side, this is particularly advantageous in situations where the optical beam quality of the laser output is poor (such as in OPG lasers) and when the optical materials under study are fragile.

ACKNOWLEDGMENTS

This work is supported by an interregional research program Bretagne-Pays de Loire: "Verres Infrarouges pour Fonctions Optiques Télécom.".

[1] S. Cherukulappurath, G. Boudebs, and A. Monteil, J. Opt. Soc. Am. B **21**, 273 (2004).
[2] M. Sheik-Bahae, A. A. Said, T. H. Wei, D. Hagan, and E. W. Stryland, IEEE J. Quantum Electron. **26**, 760 (1990).
[3] W. Zhao and P. Palffy-Muhoray, Appl. Phys. Lett. **63**, 1613 (1993).
[4] G. Boudebs, M. Chis, and X. Nguyen Phu, J. Opt. Soc. Am. B **18**, 623 (2001).
[5] G. Boudebs, F. Sanchez, C. Duverger, and B. Boulard, Opt. Commun. **199**, 257 (2001).
[6] G. Boudebs, F. Sanchez, J. Troles, and F. Smektala, Opt. Commun. **199**, 425 (2001).
[7] G. Boudebs, S. Cherukulappurath, H. Leblond, J. Troles, F. Smektala, and F. Sanchez, Opt. Commun. **219**, 427 (2003).
[8] G. Boudebs, M. Chis, and J. P. Bourdin, J. Opt. Soc. Am. B **13**, 1450 (1996).
[9] G. Boudebs, M. Chis, and A. Monteil, Opt. Commun. **150**, 287 (1998).
[10] J. W. Goodman, *Introduction to Fourier Optics*, 2nd ed. (McGraw-Hill, New York, 1996).
[11] Y. R. Shen, *Nonlinear Optics* (Wiley, New York, 1984), Chap. 3, pp. 42–50.
[12] J. A. Hermann, J. Opt. Soc. Am. B **1**, 729 (1984).
[13] W. E. Williams, M. J. Soileau, and E. W. Stryland, Opt. Commun. **50**, 256 (1984).
[14] A. Marcano, H. Maillote, D. Gindre, and D. Métin, Opt. Lett. **21**, 101 (1996).